

A Hierarchical Approach to Manipulator Velocity Field Control Considering Dynamic Friction Compensation

Javier Moreno-Valenzuela¹

Systems and Control, CITEDI-IPN,
Av. Del Parque 1310, Mesa de Otay,
Tijuana, B.C., 22510, Mexico
e-mail: moreno@citedi.mx

Rafael Kelly

CICESE, Apdo. Postal 2615,
Adm. 1, Ensenada, B.C., 22800, Mexico
e-mail: rkelly@cicese.mx

The velocity field control of robot manipulators is addressed in this paper. The proposed algorithm has a hierarchical structure based on a velocity field kinematic control scheme for joint velocity resolution and an inner loop of joint velocity control that uses an observer for friction compensation. Experiments on a two degrees-of-freedom direct-drive arm illustrate the performance of the proposed controller. [DOI: 10.1115/1.2234487]

Keywords: velocity field control, operational space, stability, friction, direct-drive robot

1 Introduction

Motion control of robot manipulators in operational space is specified in terms of a desired timed trajectory $\mathbf{y}_d(t)$ for the end-effector pose \mathbf{y} . Then the motion control aim is to ensure the limit

$$\lim_{t \rightarrow \infty} [\mathbf{y}_d(t) - \mathbf{y}(t)] = \mathbf{0}.$$

In other words, the goal is that end-effector pose $\mathbf{y}(t)$ achieves asymptotic tracking of the desired timed trajectory $\mathbf{y}_d(t)$. The motion control—or trajectory tracking control—of robot manipulators in operational space has been widely addressed in the literature. See [1] for a survey on operational space tracking control. Figure 1 illustrates the concept of trajectory tracking control.

¹Corresponding author.

Contributed by the Dynamic Systems, Measurement, and Control Division of ASME for publication in the JOURNAL OF DYNAMIC SYSTEMS, MEASUREMENT, AND CONTROL. Manuscript received September 12, 2003; final manuscript received June 10, 2005. Assoc. Editor: Michael Goldfarb.

The passive velocity field control was introduced in [2,3], and it has been reconized as an alternative to motion control [4]. In this control philosophy, the task to be accomplished by the robot is coded by a smooth desired *velocity vector field* defined in the operational configuration space \mathcal{G} and denoted as a map

$$\begin{aligned} \mathbf{v}(\mathbf{y}): \mathcal{G} &\rightarrow T\mathcal{G} \\ \mathbf{y} &\mapsto \mathbf{v}(\mathbf{y}) \end{aligned}$$

where $T\mathcal{G}$ denotes the tangent bundle of \mathcal{G} [5]. A velocity field defines a tangent vector at every point of the robot operational configuration space. Figure 1 illustrates the specification of motion by means of a velocity field. This figure depicts a velocity field defined in the three dimensional Cartesian space of a robot arm that assigns a desired velocity vector (arrow) to each point in the task space. Let us notice that in many application the timing of the desired trajectory is unimportant with respect to the coordination and synchronization requirements between the various degrees of freedom. In this way, velocity field control approach is particularly well suited to contour following tasks for machining operations such as cutting, milling, and deburring [6].

The velocity field control has been reformulated in [4] without considering closed-loop passivity requirements:

The velocity field control objective in operational space is established as the design of the torques input $\boldsymbol{\tau}$ so that

$$\lim_{t \rightarrow \infty} [\mathbf{v}(\mathbf{y}(t)) - \dot{\mathbf{y}}(t)] = \mathbf{0}, \quad (1)$$

where the difference between the desired velocity field $\mathbf{v}(\mathbf{y})$ and the manipulator end-effector velocity $\dot{\mathbf{y}}$ defines the velocity field error.

Thus, instead of requiring the arm end-effector tip to be at specific location at each instant time, as it is imposed in the trajectory tracking control, in velocity field control the arm follows out the flow lines of the desired velocity field, as can be seen in Fig. 1.

The kinematic control concept [1,7], deals with the problem of controlling the end-effector pose, assuming that the joint velocities are the robot inputs. This assumption only is allowed when a suitable joint velocity control loop is utilized. To solve the velocity field control a control strategy based on a hierarchical structure is proposed in this paper (see Fig. 1). This structure consists of using the kinematic control concept for joint velocity resolution and an asymptotically stable joint velocity controller.

The dynamics in joint space of a serial-chain n -link robot manipulator considering the presence of friction at the robot joints can be written as [1]

$$M(\mathbf{q})\ddot{\mathbf{q}} + C(\mathbf{q}, \dot{\mathbf{q}})\dot{\mathbf{q}} + \mathbf{g}(\mathbf{q}) + f(\mathbf{z}, \dot{\mathbf{q}}) = \boldsymbol{\tau} \quad (2)$$

where \mathbf{q} is the $n \times 1$ vector of joint displacements, $\dot{\mathbf{q}}$ is the $n \times 1$ vector of joint velocities, $\boldsymbol{\tau}$ is the $n \times 1$ vector of applied torque inputs, $M(\mathbf{q})$ is the $n \times n$ symmetric positive definite manipulator inertia matrix, $C(\mathbf{q}, \dot{\mathbf{q}})\dot{\mathbf{q}}$ is the $n \times 1$ vector of centripetal and Coriolis torques, $\mathbf{g}(\mathbf{q})$ is the $n \times 1$ vector of gravitational torques, and

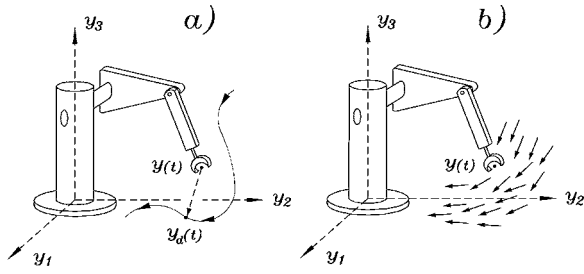


Fig. 1 (a) Trajectory tracking control in Cartesian space; (b) velocity field control in Cartesian space

$\mathbf{f}(\mathbf{z}, \dot{\mathbf{q}})$ is the $n \times 1$ vector of torques due to the friction that depends on the joint velocity $\dot{\mathbf{q}}$ and an unmeasurable internal state $\mathbf{z} \in \mathbb{R}^n$, which will be defined below.

One of the simplest dynamic models—based on a bristle deflection interpretation—is the Dahl's model [8], which, including viscous friction, can be described by

$$\dot{\mathbf{z}} = -\Psi(\dot{\mathbf{q}})\mathbf{z} + \dot{\mathbf{q}}, \quad (3)$$

$$\mathbf{f}(\mathbf{z}, \dot{\mathbf{q}}) = \Sigma_0 \mathbf{z} + F_v \dot{\mathbf{q}}, \quad (4)$$

where $F_v = \text{diag}\{f_{v_1}, \dots, f_{v_n}\}$ is a positive definite diagonal matrix that contains the viscous friction coefficient of each joint, $\Sigma_0 = \text{diag}\{\sigma_{0_1}, \dots, \sigma_{0_n}\}$ is a positive definite diagonal matrix "stiffness" parameter of each joint and

$$\Psi(\dot{\mathbf{q}}) = \text{diag} \left\{ \frac{\sigma_{0_1}}{f_{C_1}} |\dot{q}_1|, \dots, \frac{\sigma_{0_n}}{f_{C_n}} |\dot{q}_n| \right\}$$

is a positive semidefinite diagonal matrix where f_{C_i} denotes the Coulomb parameter for each joint $i = 1, \dots, n$. It can be shown that this friction model satisfies the requirements stated in [9] to get a passive operator from velocity $\dot{\mathbf{q}}$ to friction force \mathbf{f} .

Denoting $\mathbf{h}(\mathbf{q}): \mathbb{R}^n \rightarrow \mathbb{R}^m$ the robot direct kinematics ($m \leq n$), then the position and orientation $\mathbf{y} \in \mathbb{R}^m$ of the end effector is given by

$$\mathbf{y} = \mathbf{h}(\mathbf{q}). \quad (5)$$

The time derivative of the direct kinematic model (5) yields the differential kinematics

$$\dot{\mathbf{y}} = \frac{d}{dt} \mathbf{h}(\mathbf{q}) = \frac{\partial \mathbf{h}}{\partial \mathbf{q}} \dot{\mathbf{q}} = \mathbf{J}(\mathbf{q}) \dot{\mathbf{q}} \quad (6)$$

where $\mathbf{J}(\mathbf{q})$ is the so-called analytical Jacobian matrix [1]. In this paper the analytical Jacobian $\mathbf{J}(\mathbf{q})$ is assumed of full-rank (rank = m) and bounded by k_J , i.e.,

$$\|\mathbf{J}(\mathbf{q})\| \leq k_J, \quad \forall \mathbf{q} \in \mathbb{R}^n. \quad (7)$$

This paper is organized as follows. In Sec. 2 we deal with velocity field control for robot manipulators. In Sec. 3, experimental results carried out on a direct-drive robot arm are shown. Finally, some concluding remarks are drawn in Sec. 4.

Throughout this paper the following notation will be adopted. $\|\mathbf{x}\| = \sqrt{\mathbf{x}^T \mathbf{x}}$ stands for the norm of vector $\mathbf{x} \in \mathbb{R}^n$. $\lambda_m\{A(\mathbf{x})\}$ and $\lambda_M\{A(\mathbf{x})\}$ denote the minimum and maximum eigenvalues of a symmetric positive definite matrix $A(\mathbf{x}) \in \mathbb{R}^{n \times n}$ for all $\mathbf{x} \in \mathbb{R}^n$, respectively.

2 Velocity Field Control

2.1 Velocity Field Kinematic Control. In this paper we assume that the desired velocity field $\mathbf{v}(\mathbf{y})$ is bounded in the sense that

$$\|\mathbf{v}(\mathbf{y})\| \leq \|\mathbf{v}\|_M, \quad \forall \mathbf{y} \in \mathbb{R}^m, \quad (8)$$

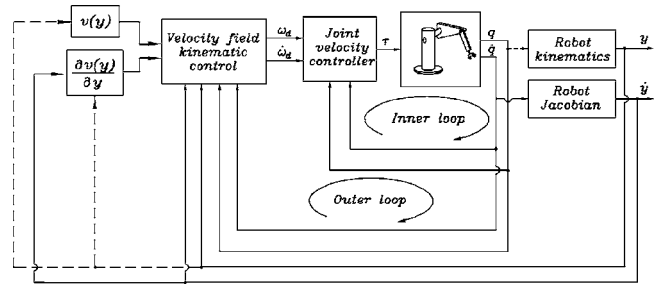


Fig. 2 Block diagram of the hierarchical velocity field control

where $\|\mathbf{v}\|_M$ is a strictly positive constant.

Under the optics of kinematic control, the joint velocity $\dot{\mathbf{q}}$ is considered as the input for the system given by the differential kinematics (6). In virtue that the robot Jacobian $\mathbf{J}(\mathbf{q})$ was assumed full-rank and bounded, we proposed the following control law to generate the desired joint velocity ω_d

$$\omega_d = \mathbf{J}(\mathbf{q})^T [\mathbf{v}(\mathbf{y}) + \mathbf{K}\rho], \quad (9)$$

$$\dot{\rho} = \mathbf{v}(\mathbf{y}) - \dot{\mathbf{y}}, \quad (10)$$

where \mathbf{K} is an $m \times m$ symmetric positive definite matrix. Suppose momentarily that the robot at hand is equipped with an ideal joint velocity control system guaranteeing that the actual joint velocity $\dot{\mathbf{q}}$ matches the desired joint velocity ω_d , i.e.,

$$\dot{\mathbf{q}}(t) \equiv \omega_d(t). \quad (11)$$

Then, substituting (9) into (6) leads to

$$\dot{\rho} = -\mathbf{K}\rho.$$

Because \mathbf{K} is a symmetric positive definite matrix, then exponential vanishing of the velocity field error is guaranteed, i.e., the limit (1) is attained. Thus, the control law (9) and (10) will guarantee the velocity field control objective as long as the velocity matching assumption (11) holds.

However, most of velocity controllers used in practice assure—in the best case—only asymptotic velocity tracking instead of exact tracking. The consequence of this fact is that the velocity matching assumption (11) may fail in practice depending on the manipulator servo system and the range of requested desired joint velocity ω_d . Let us define the joint velocity error as $\tilde{\omega} = \omega_d - \dot{\mathbf{q}}$. Thus, the velocity field error dynamics results

$$\dot{\rho} = -\mathbf{K}\rho + \mathbf{J}(\mathbf{q})\tilde{\omega}. \quad (12)$$

Practical implementation of the kinematic velocity field control law (9) and (10) requires the design of a joint velocity controller. The resulting control structure is named hierarchical velocity field control. See Fig. 2 for a block diagram.

2.2 Inner Loop Based on PD Control With Compensation.

Inspired in the PD control with compensation, derived from the nonadaptive version of the motion controller proposed by Slotine and Li [10], the following joint velocity controller has been introduced in [11]:

$$\tau = \mathbf{M}(\mathbf{q})[\dot{\omega}_d + \Lambda \tilde{\omega}] + \mathbf{C}(\mathbf{q}, \dot{\mathbf{q}})[\omega_d + \Lambda \tilde{\xi}] + \mathbf{g}(\mathbf{q}) + \mathbf{K}_v \tilde{\omega} + \mathbf{K}_i \tilde{\xi} + F_v \dot{\mathbf{q}} + \Sigma_0 \hat{\mathbf{z}} \quad (13)$$

$$\dot{\xi} = \tilde{\omega} \quad (14)$$

where \mathbf{K}_i and \mathbf{K}_v denote $n \times n$ definite positive matrices, $\Lambda = \mathbf{K}_v^{-1} \mathbf{K}_i$, the desired joint velocity ω_d is given in (9), and $\hat{\mathbf{z}}$ is an estimation of the internal state \mathbf{z} of the friction model (3) and (4). The corresponding observer for $\hat{\mathbf{z}}$ is described by

$$\dot{\hat{\mathbf{z}}} = -\Psi(\dot{\mathbf{q}})\hat{\mathbf{z}} + \omega_d + \Lambda \tilde{\xi}. \quad (15)$$

The closed-loop system is obtained by substituting the controller (13) and (14) into the robot model (2)–(4), and utilizing the velocity field error dynamics (12) yields

$$\frac{d}{dt} \begin{bmatrix} \boldsymbol{\rho} \\ \boldsymbol{\xi} \\ \tilde{\boldsymbol{\omega}} \\ \tilde{\mathbf{z}} \end{bmatrix} = \begin{bmatrix} -K\boldsymbol{\rho} + J(\mathbf{q})\tilde{\boldsymbol{\omega}} \\ \tilde{\boldsymbol{\omega}} \\ M(\mathbf{q})^{-1}[-C(\mathbf{q}, \dot{\mathbf{q}})[\tilde{\boldsymbol{\omega}} + \Lambda\boldsymbol{\xi}] - K_v\tilde{\boldsymbol{\omega}} - K_i\boldsymbol{\xi} - \Sigma_0\tilde{\mathbf{z}}] - \Lambda\tilde{\boldsymbol{\omega}} \\ -\Psi(\dot{\mathbf{q}})\tilde{\mathbf{z}} + \tilde{\boldsymbol{\omega}} + \Lambda\boldsymbol{\xi} \end{bmatrix} \quad (16)$$

where $\tilde{\mathbf{z}} = \hat{\mathbf{z}} - \mathbf{z}$ is the observation error of the internal state \mathbf{z} . An equilibrium point of the nonlinear and nonautonomous system (16) is the state space origin. Motivated by the analysis presented in [12], we propose the following Lyapunov function

$$V(\boldsymbol{\rho}, \boldsymbol{\xi}, \tilde{\boldsymbol{\omega}}, \tilde{\mathbf{z}}) = \frac{1}{2}[\tilde{\boldsymbol{\omega}} + \Lambda\boldsymbol{\xi}]^T M(\mathbf{q})[\tilde{\boldsymbol{\omega}} + \Lambda\boldsymbol{\xi}] + \boldsymbol{\xi}^T K_i \boldsymbol{\xi} + \frac{1}{2}\tilde{\mathbf{z}}^T \Sigma_0 \tilde{\mathbf{z}} + \alpha \boldsymbol{\rho}^T \boldsymbol{\rho},$$

where

$$\frac{4\lambda_m\{K_v\}\lambda_m\{K\}}{k_f^2} > \alpha > 0, \quad (17)$$

This is a globally positive definite function as well as radially unbounded and decrescent. After some algebra, we have that the time derivative of $V(\boldsymbol{\rho}, \boldsymbol{\xi}, \tilde{\boldsymbol{\omega}}, \tilde{\mathbf{z}})$ along the trajectories of the closed-loop system (16) is

$$\dot{V}(\boldsymbol{\rho}, \boldsymbol{\xi}, \tilde{\boldsymbol{\omega}}, \tilde{\mathbf{z}}) = -\tilde{\boldsymbol{\omega}}^T K_v \tilde{\boldsymbol{\omega}} - \boldsymbol{\xi}^T K_i K_v^{-1} K_i \boldsymbol{\xi} - \tilde{\mathbf{z}}^T \Sigma_0 \Psi(\dot{\mathbf{q}})\tilde{\mathbf{z}} - \alpha \boldsymbol{\rho}^T K \boldsymbol{\rho} + \alpha \boldsymbol{\rho}^T J(\mathbf{q})\tilde{\boldsymbol{\omega}}.$$

Taking an upper bound on $\dot{V}(\boldsymbol{\rho}, \boldsymbol{\xi}, \tilde{\boldsymbol{\omega}}, \tilde{\mathbf{z}})$ we obtain

$$\dot{V}(\boldsymbol{\rho}, \boldsymbol{\xi}, \tilde{\boldsymbol{\omega}}, \tilde{\mathbf{z}}) \leq - \underbrace{\begin{bmatrix} \|\tilde{\boldsymbol{\omega}}\| \\ \|\boldsymbol{\xi}\| \\ \|\boldsymbol{\rho}\| \end{bmatrix}^T \begin{bmatrix} \lambda_m\{K_v\} & 0 & -\alpha\frac{1}{2}k_f \\ 0 & \lambda_m\{K_i K_v^{-1} K_i\} & 0 \\ -\alpha\frac{1}{2}k_f & 0 & \alpha\lambda_m\{K\} \end{bmatrix} \begin{bmatrix} \|\tilde{\boldsymbol{\omega}}\| \\ \|\boldsymbol{\xi}\| \\ \|\boldsymbol{\rho}\| \end{bmatrix}}_Q. \quad (18)$$

It should be noticed that inequality (18) has been obtained and the virtue that $\Sigma_0 \Psi(\dot{\mathbf{q}})$ is positive semidefinite and using the bounded robot Jacobian assumption (7). The matrix Q in (18) is positive definite if and only if inequality (17) is satisfied. Because α can be always chosen so that $\dot{V}(\boldsymbol{\rho}, \boldsymbol{\xi}, \tilde{\boldsymbol{\omega}}, \tilde{\mathbf{z}})$ is globally negative semidefinite, and invoking the Lyapunov direct method [13], the origin of the state space of (16) is a uniformly stable equilibrium. Because $V(\boldsymbol{\rho}, \boldsymbol{\xi}, \tilde{\boldsymbol{\omega}}, \tilde{\mathbf{z}})$ is radially unbounded, the functions $\boldsymbol{\rho}, \boldsymbol{\xi}, \tilde{\boldsymbol{\omega}}, \tilde{\mathbf{z}} \in L_\infty^n$, which together with inequality (8), and the assumption of bounded robot Jacobian $J(\mathbf{q})$, implies that $\dot{\boldsymbol{\rho}}, \dot{\boldsymbol{\xi}}, \dot{\tilde{\boldsymbol{\omega}}}, \dot{\tilde{\mathbf{z}}} \in L_\infty^n$. Besides, integrating inequality (18) with respect to time it is possible to show that $\boldsymbol{\rho}, \boldsymbol{\xi}, \tilde{\boldsymbol{\omega}} \in L_2^n$. Finally, the conclusion $[\boldsymbol{\rho}(t)^T \boldsymbol{\xi}(t)^T \tilde{\boldsymbol{\omega}}(t)^T]^T \rightarrow \mathbf{0}$ as $t \rightarrow \infty$ is derived by invoking the fact that a bounded and square

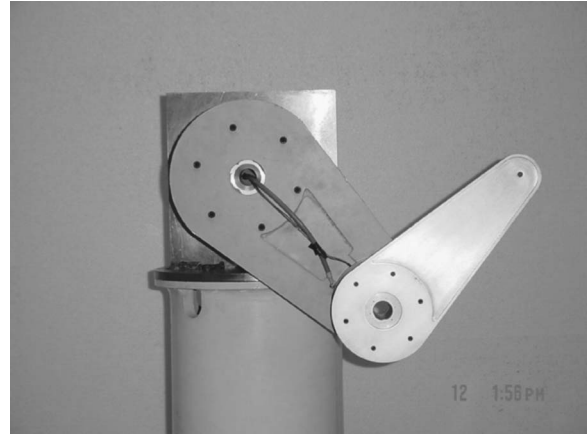


Fig. 3 Experimental arm

integrable function whose time derivative is also bounded must tend to zero. Therefore, the asymptotic vanishing of $\boldsymbol{\rho}(t)$ and $\boldsymbol{\omega}(t)$, together with the assumption of bounded robot Jacobian, assure that—see Eq. (12)—

$$\lim_{t \rightarrow \infty} \dot{\boldsymbol{\rho}}(t) = \lim_{t \rightarrow \infty} [\mathbf{v}(\mathbf{y}(t)) - \dot{\mathbf{y}}(t)] = \mathbf{0}.$$

We have shown that the velocity field control objective (1) is satisfied using the hierarchical controller (9) and (10) and (13)–(15).

3 Experimental Evaluation

The experiments presented in this section have been carried out on a mechanical arm built at the CICESE Research Center. This is a direct-drive vertical arm with two degrees of freedom whose rigid links are joined with revolute joints—see Fig. 3—. In [11] a detailed description of this experimental setup, including the estimated parameters of the Dahl friction model, as well as experimental evidence that the Dahl model captures the real behavior of the friction in the robot actuators, is introduced.

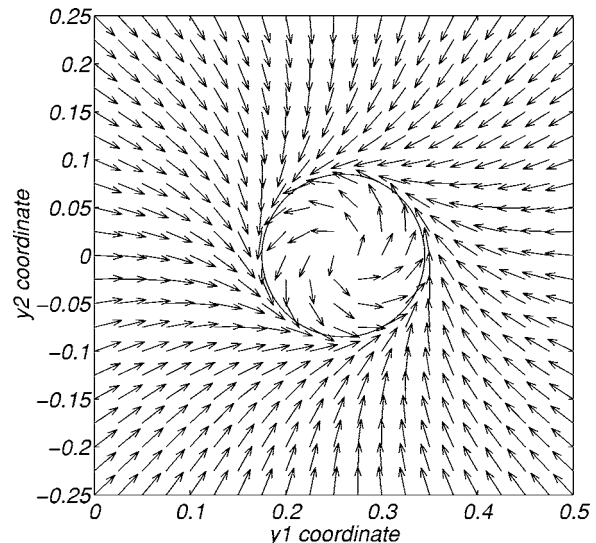


Fig. 4 Desired velocity field used in experiments

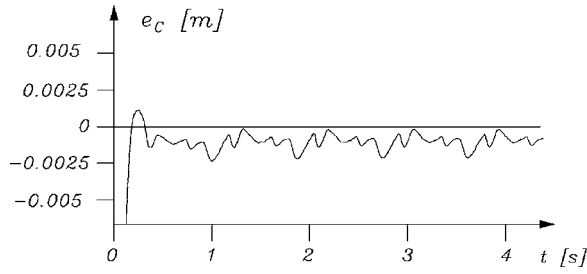


Fig. 5 PD with compensation+viscous friction compensation: Contouring error

The proposed velocity field $\mathbf{v}(\mathbf{y})$ “draws” a circle in the $y_1 - y_2$ plane, as shown in Fig. 4, where the corresponding desired speed at each point is approximately 0.65 (m/s). The control aim is to drive the arm in such a way that the position of the arm tip follows the velocity field, hence to track asymptotically a circle.

Since position error has nonsense in velocity field control, we have recurred to the contouring error to assess the performance of the velocity field controller. The contouring error is defined as [14]

$$e_c(t) = r_0 - \sqrt{[y_{c1} - y_1(t)]^2 + [y_{c2} - y_2(t)]^2},$$

where $y_{c1}=0.26$ (m) and $y_{c2}=0.0$ (m) are the circle center coordinates and $r_0=0.085$ (m) is the radius. The initial position of the robot was $[q_1(0), q_2(0)]^T = [60, 100]^T$ (deg).

In order to compare the performance of the Dahl-based joint velocity controller (13) and (14) we also present experiments using the compensation of only viscous friction. This yields the following PD with a compensation based controller

$$\begin{aligned} \boldsymbol{\tau} = & M(\mathbf{q})[\dot{\boldsymbol{\omega}}_d + \Lambda \tilde{\boldsymbol{\omega}}] + C(\mathbf{q}, \dot{\mathbf{q}})[\boldsymbol{\omega}_d + \Lambda \tilde{\boldsymbol{\xi}}] + \mathbf{g}(\mathbf{q}) + K_v \tilde{\boldsymbol{\omega}} + K_f \tilde{\boldsymbol{\xi}} \\ & + F_v \dot{\mathbf{q}}, \end{aligned} \quad (19)$$

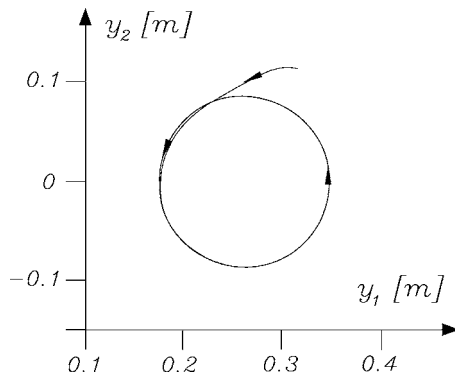


Fig. 6 PD with compensation+viscous friction compensation: Cartesian robot path

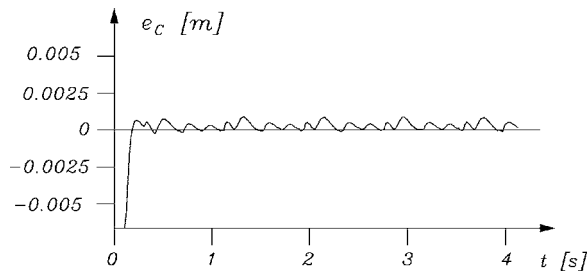


Fig. 7 PD with compensation+Dahl-based friction compensation: Contouring error

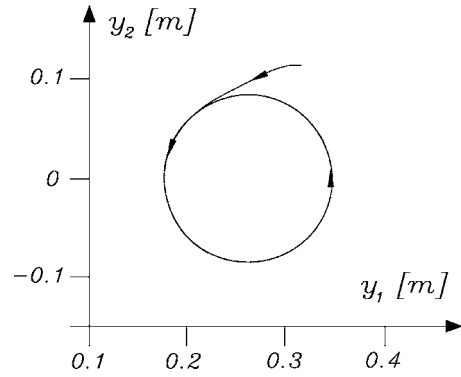


Fig. 8 PD with compensation+Dahl-based friction compensation: Cartesian robot path

$$\dot{\boldsymbol{\xi}} = \tilde{\boldsymbol{\omega}}. \quad (20)$$

The gain for the kinematic control was set to $K = \{10.0, 10.0\} \times (1/s)$. For the velocity controllers, the control gains were $K_i = \text{diag}\{100.0, 400.0\} (1/s^2)$, and $K_v = \text{diag}\{15.0, 40.0\} (1/s)$. The results of the implementation of the kinematic velocity field control (9) and (10) with the joint velocity controller (19) and (20), which uses only the compensation of viscous friction, are shown in Figs. 5 and 6. They show the contouring error and the Cartesian robot path. On the other hand, the results corresponding to kinematic velocity field control (9) and (10) with the joint velocity controller (13) and (14), which considers Dahl-based friction compensation, are shown in Fig. 7 that depict the contouring error, and Fig. 8, where the Cartesian robot path is drawn. Both experiments show good following of the desired velocity field since the arm tip is successfully guided toward the circular contour. In steady state, the peak value of the contouring error is 0.0024 (m) for viscous friction compensation, and 0.00086 (m) for Dahl-based friction compensation. Using the latter controller, the performance is enhanced by 64.16% with respect to the former. This shows the advantage of using friction compensation based on the Dahl model.

4 Summary

To solve the velocity field control objective, a hierarchical structure of kinematic control for the resolution of desired joint velocity and an asymptotically joint velocity controller with friction compensation was proposed. Experimental results showed that the compensation of friction based on the Dahl model presents better performance than the compensation of only viscous friction.

Acknowledgment

This work was partially supported by CONACyt, Mexico.

References

- [1] Canudas de Wit, C., Siciliano, B., and Bastin, G., 1996, in *Theory of Robot Control*, Springer-Verlag, London.
- [2] Li, P. Y., and Horowitz, R., 1999, “Passive Velocity Field Control of Mechanical Manipulators,” *IEEE Trans. Rob. Autom.*, **15**, pp. 751–763.
- [3] Li, P. Y., and Horowitz, R., 2001, “Passive Velocity Field Control (PVFC): Part I—Geometry and Robustness,” *IEEE Trans. Autom. Control*, **46**, pp. 1346–1359.
- [4] Moreno, J., and Kelly, R., 2002, “On Manipulator Control Via Velocity Fields,” *Proc. 15th IFAC World Congress*, Barcelona, Spain.
- [5] Murray, R. M., Li, Z., and Sastry, S. S., 1994, *A Mathematical Introduction to Robotic Manipulation*, CRC Press, Boca Raton, FL.
- [6] Li, P. Y., 1999, “Coordinated Contour Following Control for Machining Operations—A Survey,” *Proc. of the American Control Conference*, San Diego, CA, pp. 4543–4547.

- [7] Siciliano, B., 1990, "Kinematic Control of Redundant Robot Manipulators: A Tutorial," *J. Intell. Robotic Syst.*, **3**, pp. 201–212.
- [8] Dahl, P. R., 1976, "Solid Friction Damping of Mechanical Vibrations," *AIAA J.*, **14**, pp. 1675–1682.
- [9] Barabanov, N., and Ortega, R., 2000, "Necessary and Sufficient Conditions for Passivity of the LuGre Friction Model," *IEEE Trans. Autom. Control*, **45**, pp. 830–832.
- [10] Slotine, J., and Li, W., 1988, "Adaptive Manipulator Control: A Case Study," *IEEE Trans. Autom. Control*, **33**, pp. 995–1003.
- [11] Moreno, J., Kelly, R., and Campa, R., 2003, "Manipulator Velocity Control Using Friction Compensation," *IEE Proc.: Control Theory Appl.*, **150**, pp. 119–126.
- [12] Spong, M. W., Ortega, R., and Kelly, R., 1990, "Comments on 'Adaptive Manipulator Control: A Case Study'," *IEEE Trans. Autom. Control*, **35**, pp. 761–762.
- [13] Vidyasagar, M., 1993, *Nonlinear Systems Analysis*, Prentice-Hall, Englewood Cliffs, NJ.
- [14] Chiu, G. T.-C., and Tomizuka, M., 2001, "Contouring Control of Machine Tool Feed Drive Systems: A Task Coordinate Frame Approach," *IEEE Trans. Control Syst. Technol.*, **9**, pp. 130–131.